Real-time quantitative optical method to study temperature dependence of crack propagation process in colloidal photonic crystal film*

Lin Dong-Feng(林冬风)[a)b)], Xu Yu-Zhuan(徐余颛)[a)b)], Shi Jiang-Jian(石将建)[a)b)], Zhang Yu(张 瑜)[a)b)], Luo Yan-Hong(罗艳红)[a)b)], Li Dong-Mei(李冬梅)[a)b)†], and Meng Qing-Bo(孟庆波)[a)b)‡]

[a)] *Key Laboratory for Renewable Energy, Chinese Academy of Sciences, Beijing* 100190, *China*
[b)] *Beijing Key Laboratory for New Energy Materials and Devices, Institute of Physics, Chinese Academy of Sciences, Beijing* 100190, *China*

(Received 25 March 2015; revised manuscript received 16 April 2015; published online 29 May 2015)

A real-time quantitative optical method to characterize crack propagation in colloidal photonic crystal film (CPCF) is developed based on particle deformation models and previous real-time crack observations. The crack propagation process and temperature dependence of the crack propagation rate in CPCF are investigated. By this method, the crack propagation rate is found to slow down gradually to zero when cracks become more numerous and dense. Meanwhile, with the temperature increasing, the crack propagation rate constant decreases. The negative temperature dependence of the crack propagation rate is due to the increase of van der Waals attraction, which finally results in the decrease of resultant force. The findings provide new insight into the crack propagation process in CPCF.

Keywords: colloidal photonic crystal, crack propagation, temperature, real-time quantitative optical method

PACS: 78.67.–n, 62.20.mt **DOI:** 10.1088/1674-1056/24/7/077803

1. Introduction

Cracks exist commonly in drying colloidal films,[1–11] clays,[12,13] and paintings.[14–16] They not only can influence the rigidity and quality of materials, but also can be applied to identify the age, origin, and art forgery of paintings.[14–16] Cracking in drying colloidal photonic crystal film (CPCF) is one of representative phenomena and attracts the attention of researchers all over the world.[3,4,6,8–10,17] In theoretical studies, efforts are mainly devoted to investigating the mechanism and building models of crack propagation, including stick-slip motion[8] and particle deformation models.[5,7,17] Some models based on particle deformation have been set up, suggesting that particle deformation resulting in cracks is caused by different forces, such as surface tension, van der Waals, and tensile stress. However, these models emphasize on the critical time when cracks propagate in the film, while a whole crack propagation process is little investigated.

In experimental studies, efforts are mainly devoted to the final states of crack such as types[1] and spacing.[3,6] Recently, Routh[6] and Wang[3] found that the final crack spacing increases when the temperature increases[6] or the particle radius decreases.[3] However, crack spacing is not suitable for characterizing cracks when the cracks are not parallel. Because of the lack of a real-time quantitative method for crack measurement, the crack propagation process remains unrevealed. Moreover, further detailed insight into the temperature dependence of the crack propagation rate is still unclear. Thus, real-time quantitative studies on the crack propagation process and the influence of temperature on crack propagation rate are essential for understanding the mechanism of this process.

In our previous work,[18–20] an experimental method for CCD observation and reflectance measurement of the crack propagation was developed. In the present work, a real-time quantitative optical method is developed to characterize cracking in CPCFs. The detailed relationship between particle deformation value and the reflectance red-shift is built. Then the crack propagation process is investigated by this method in real time. Finally, the temperature dependence of the crack propagation rate is also investigated.

2. Materials and methods

The experimental set-up, materials, and investigation procedure follow our previous work reported in Ref. [18]. Simply speaking, colloidal photonic crystal films were fabricated from 1 vol.% aqueous suspensions of 240-nm polystyrene (PS) latex through evaporation-induced colloidal self-assembly. A CCD camera and monochromator were used synchronously to obtain real-time *in-situ* CCD images and reflectance spectra of CPCF. The further development in this experiment was that hot air streams at different temperatures (ranging from 100

*Project supported by the National Basic Research Program of China (Grant Nos. 2012CB932903 and 2012CB932904) and the National Natural Science Foundation of China (Grant Nos. 51372270, 11474333, and 21173260).

†Corresponding author. E-mail: dmli@iphy.ac.cn

‡Corresponding author. E-mail: qbmeng@iphy.ac.cn

© 2015 Chinese Physical Society and IOP Publishing Ltd

to 180 °C) were set to investigate the influence of temperature. The local temperatures around the monitored CPCF region were 44.8, 47, 50.7, 57.6, and 63.9 °C, respectively.

3. Results and discussion

3.1. Real-time quantitative crack characterization from reflectance spectrum red-shift: particle deformation value

As shown in Fig. 1, along with crack propagating throughout CPCF, the peak positions of reflectance spectra shift to longer wavelengths (red-shift). These two macroscopic processes, crack propagation[5,7,17] and reflectance spectrum red-shift,[18] are both found to be related to microcosmic particle deformation. On one hand, the spherical particles are observed by SEM to have deform to polyhedral particles,[21–23] and the particle deformation results in crack propagation during drying.[5,7,17] On the other hand, the interstices between particles decrease due to the shape change from spherical to polyhedral.[22,23] The decrease of interstices results in the increase of particle volume fraction and then the red-shift of reflectance spectrum peak positions.[18] Therefore, the particle deformation is the connection between crack propagation and reflectance spectrum red-shift. When particles deform more seriously, more cracks are found propagating with higher density. The particle deformation value is the appropriate parameter to characterize cracks quantitatively, including the interfacial and inside cracks. What one needs to do first is to derive the particle deformation value from the reflectance spectrum red-shift. A detailed derivation follows.

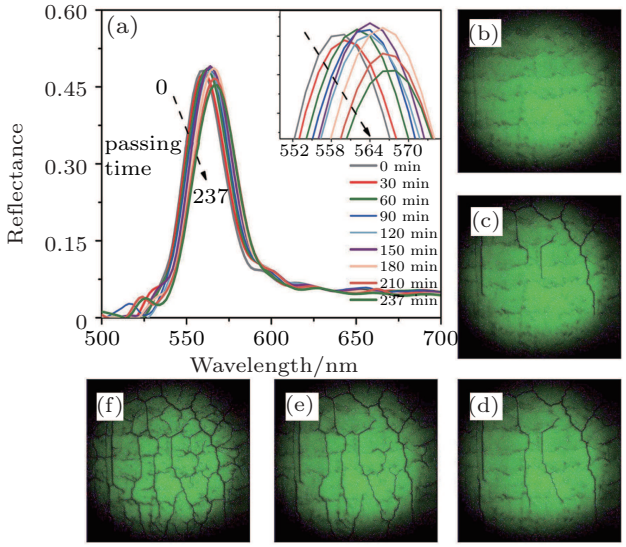


Fig. 1. (color online) Real-time *in-situ* evolution of CPCF (a) reflectance spectra and (b)–(f) CCD images in CPCF during crack propagation.

Many experiments and simulations have revealed that mono-dispersed PS spherical particles self-assemble into a face-centered cubic (FCC) structure with the (111) planes parallel to the substrate interface during vertical deposition. The diffracted wavelength (λ) is given by the Bragg equation[24]

$$m\lambda = 2d_{111}\sqrt{n_{\text{eff}}^2 - \sin^2\theta}, \tag{1}$$

where m is the diffraction order, d_{111} is the inter-planar spacing of (111) planes, n_{eff} is the effective refractive index of the crystal, and θ is the incident angle. Here, θ is zero when the incident light is normal to the substrate interface. The effective refractive index of the crystal n_{eff} is given by a volume-weighted average,

$$n_{\text{eff}} = \sqrt{\phi_{\text{particle}} n_{\text{particle}}^2 + \phi_{\text{water}} n_{\text{water}}^2 + (1 - \phi_{\text{particle}} - \phi_{\text{water}}) n_{\text{air}}^2}, \tag{2}$$

where ϕ_{particle} and ϕ_{water} are the volume fractions occupied by PS particles and water between the particles, respectively. When m is 1, λ is the peak-position wavelength of reflectance spectrum.

With the solvent evaporating, PS particles start to deform, the particle distance and the interstices between particles decrease,[22,23] resulting in the change of $\varphi_{\text{particle}}$ and λ.[18] To compute ϕ_{particle} simply in our system, three assumptions are made here. First, CPCF is nearly dried out and ϕ_{water} is regarded as zero during the deformation. Secondly, the time when the cracks begin to propagate and the reflectance spectrum begins to red-shift, is defined as zero time. At this time, CPCF is compact and ϕ_{particle} is 0.74. The adjacent particle distance at this time is defined as R_0 and can be obtained from substituting initial experimental λ into Eqs. (1) and (2). Third, particle deformation is anisotropic due to the transverse shear stress, and the average of particle distance is considered and defined as R. The change of inter-plane spacing d_{111} is considered to be small during deformation, and d_{111} equals $(2/3)^{1/2}R_0$.

The lattice constant a equals $2^{1/2}R$ and the volume of a unit cell V_{cell} equals $(2^{1/2}R)^3$. When the particle distance R decreases, V_{cell} decreases as well. There are four particle spheres in one unit cell and the total volume of particle spheres V_{particle} equals $4(4/3)\pi(R_0/2)^3$. During the deformation, the total volume of spheres V_{particle} does not change, and thus $\varphi_{\text{particle}}$ becomes

$$\begin{aligned}\varphi_{\text{particle}} &= \frac{V_{\text{particle}}}{V_{\text{cell}}} \\ &= \frac{4(4/3)\pi(R_0/2)^3}{a^3} \\ &= \frac{4(4/3)\pi(R_0/2)^3}{(\sqrt{2}R)^3} = \frac{\pi}{3\sqrt{2}}\left(\frac{R_0}{R}\right)^3.\end{aligned} \tag{3}$$

After solving Eqs. (1)–(3) simultaneously, the relationship between λ and R is obtained. Further substituting the experimental peak-position wavelength λ at various times into Eqs. (1)–(3), R at various times are obtained. The difference

value of R with respect to R_0 is the particle deformation value D. Figures 2(a)–2(c) present the evolution of experimental peak-position wavelength λ, particle distance R, and particle deformation value D. As shown in Figs. 1 and 2, crack propagates when reflectance spectrum peak-position wavelength λ increases. Meanwhile, the particle distance R decreases and particle deformation value D increases. That is, when the particle deforms more seriously, the crack increases and becomes denser. The particle deformation value characterizes the crack, and the particle deformation process characterizes the crack propagation process.

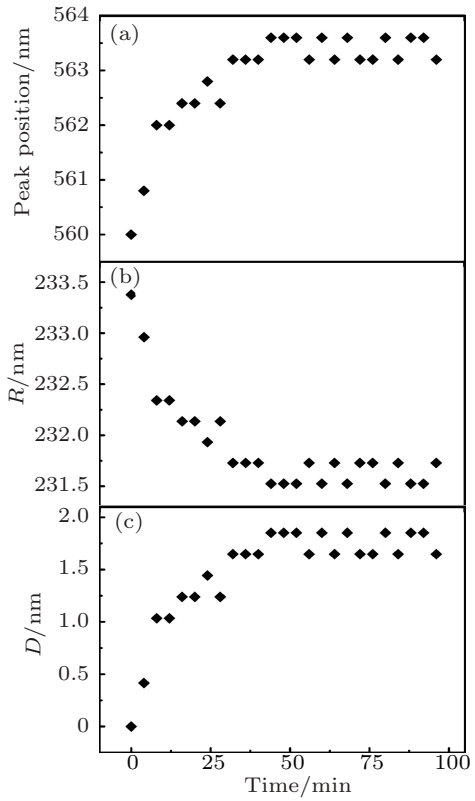


Fig. 2. Evolution of (a) peak-position wavelength λ in experimental reflection spectra, (b) particle distance R derived from Eqs. (1)–(3), (c) particle deformation value D.

3.2. Real-time particle deformation and crack propagation processes

As shown in Fig. 2(b), the particle distance R decreases and then keeps constant as time goes on. The particle deformation value D increases when the crack propagates. The absolute value of the R–t curve slope, which is defined as deformation rate v, decreases with time. As D is the change of R, v is also the slope of D–t curve. To obtain the regularity of the particle deformation rate, the relationship between R and v is first established and analyzed by statistical fitting analysis.

As the experimental temperatures are below the glass transition temperature of PS ($T_g = 98.71$ °C shown in Fig. A1 of Appendix A), the particle deformation process is mainly controlled by van der Waals attraction and tensile stress in the drying film.[7] Van der Waals attraction keeps the particles together, whereas tensile stress arising from the particle deformation repulses the particles. Tensile stress is larger than van der Waals attraction; thus the direction of the resultant force is opposite to that of v; v is slowed down by the resultant force F and is a function of F, represented as $v = f(F)$. Meanwhile, van der Waals and tensile stress both relate to R, and thus the resultant force F is a function of R, represented as $F = f(R)$. Therefore, v is a function of R and represented as $v = f(R)$. From the evolution of R and v in Fig. 2(b), v correlates with R. The relationship between them can be written as

$$v \propto R^n, \tag{4}$$

where $n \geq 0$, which is undetermined. As R keeps constant after a period of time, a modified value R_∞ is introduced and the relationship between R and v is represented as

$$v = k(R - R_\infty)^n, \tag{5}$$

where R_∞ is the particle distance at infinite time, k is the deformation rate constant, and R is the particle distance at time t.

In terms of $v = \mathrm{d}R/\mathrm{d}t$, equation (5) becomes

$$v = k(R - R_\infty)^n = \frac{\mathrm{d}R}{\mathrm{d}t}. \tag{6}$$

To obtain the specific relationship between R and t, n should be determined first. Considering that this is a microdeformation process, n is suggested to be an integer. Based on statistical theory, n is finally determined to be one by the trial-and-error method. The detailed analysis and correlation test are shown in Appendix B. Then the integration of R and t is performed and the specific relationship between R and t is

$$R = \Delta R\, \mathrm{e}^{kt} + R_\infty, \tag{7}$$

where ΔR equals $(R_0 - R_\infty)$, and R_0 is the particle distance at zero time. The fitting curves and relations are shown in Figs. 3(a)–3(e).

As shown in Fig. 3 and Eqs. (4)–(7), the fitting results show that the particle deformation rate v has a first-order correlation to R. With time going by, particle distance R decreases gradually, and the deformation rate v decreases as well. This is due to the existence of repulsive resultant force when the particles deform seriously. That is, when the particle deformation value D increases, the deformation rate v decreases. In macroscopic terms, the crack propagation rate slows down when the cracks become more numerous and denser. After a period of time, the deformation rate v stays stable and the crack propagation stops. This agrees intuitively with the CCD image evolution of crack.

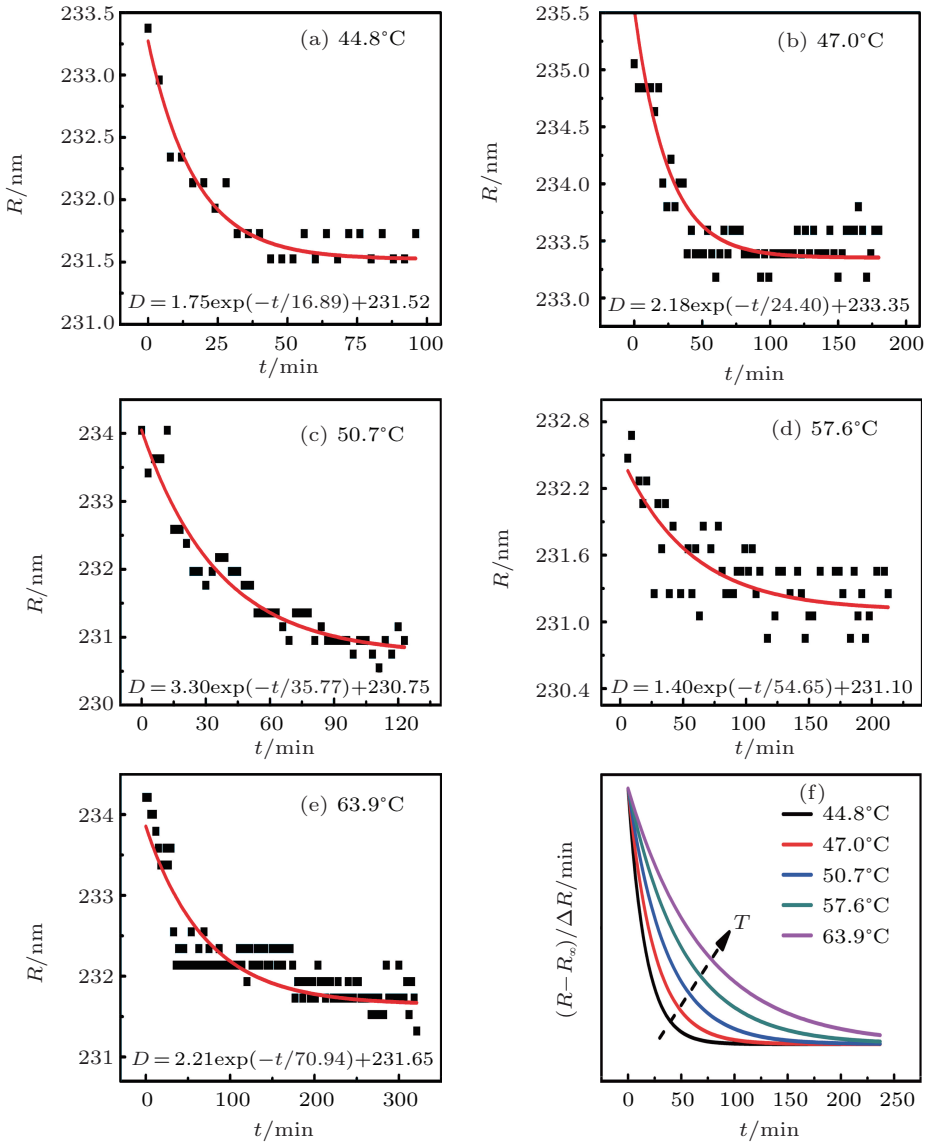


Fig. 3. (color online) (a)–(e) Experimental (black dot) and fitting (red line) evolution of particle distance D at different temperatures. (a) 44.8 °C, (b) 47 °C, (c) 50.7 °C, (d) 57.6 °C, (e) 63.9 °C. (f) Fitting curves of normalized particle distance D with t at different temperatures.

3.3. Temperature dependence of particle deformation and crack propagation processes

To compare the tendencies of crack propagation processes at different temperatures, normalized R is plotted against t in Fig. 3(f). As shown in Fig. 3(f), the particle deformation process proceeds more slowly when temperature increases. This tendency is also reflected in the rate constant k. In Figs. 3(a)–3(e), the rate constant k is negative due to the reaction direction; thus, the absolute values of k are considered here; $|k|$ at different temperatures is obtained from the fitting curves, and the temperature dependence of $|k|$ is plotted in Fig. 4. When the temperature increases, $|k|$ decreases, indicating that the deformation rate decreases under the same conditions. The particle deformation process exhibits negative temperature dependence.

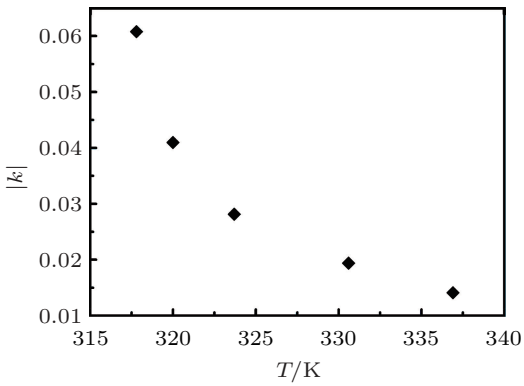


Fig. 4. Absolute variation of deformation rate constant $|k|$ with temperature T.

The negative temperature dependence of the deformation rate can be explained as follows. As mentioned above, the resultant force F is opposite to v, and v slows down. When the temperature increases between 317.9 K and 337.1 K, van der Waals attraction increases, according to Ref. [25]. However, the tensile stress does not change, and thus the resul-

tant force F decreases. The estimation of the magnitude of forces is shown in Appendix C. The decrease of resultant force F finally results in the decrease of deformation rate constant. When the temperature increases, the deformation rate changes more slowly, and the deformation rate constant decreases. In macroscopic terms, the crack propagation rate constant slows down as temperature increases, which suggests that the crack propagation rate is negatively dependent upon temperature. Meanwhile, fewer cracks are observed (as shown in Fig. D1 in Appendix D, in agreement with the result described in Ref. [6] that the final crack spacing increases with increasing temperature.

Therefore, in order to achieve high quality CPCFs and reduce cracking, a certain higher temperature is preferred in drying films. These results provide a real-time quantitative way to help get deeper insight into the crack propagation mechanism, and then to control crack propagation. The detailed mechanism and theoretical analysis of crack propagation still needs to be systematically researched in further work.

4. Conclusions

A real-time quantitative optical method, the colloidal particle deformation value derived from reflectance spectra, is developed to investigate the crack propagation process. The crack propagation rate is found to slow down gradually to zero when cracks propagate. Moreover, a negative temperature dependence of the crack propagation rate is found after changing the temperature. With the temperature increasing, the crack propagation rate constant decreases. Detailed investigation reveals that the variation of the crack propagation rate constant is due to the increase of van der Waals attraction between particles, finally resulting in a decrease of resultant force. The method and findings provide new insight into the crack propagation process, which may help improve the manufacturing method and then the quality of materials.

Appendix A: DSC curve of PS colloids

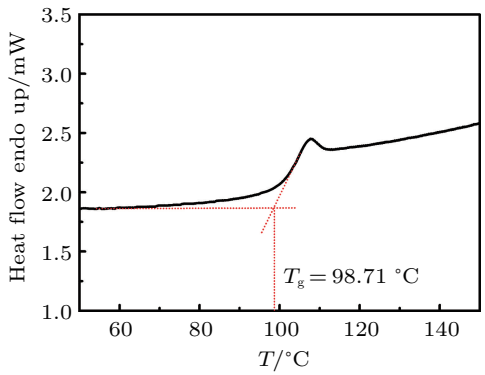


Fig. A1. (color online) DSC curve of PS colloids.

Appendix B: detail analysis and correlation test to determine the value of *n*

Considering the particle deformation process is a microcosmic process, n is suggested as an integer and is determined by the trial-and-error method here. To simplify the problem, n is tried as 0, 1, and 2 below.

When $n = 0$, equation (6) becomes

$$v = k(R - R_\infty)^0 = k = \frac{\mathrm{d}R}{\mathrm{d}t}. \tag{B1}$$

Do integration of R and t and the specific relationship between R and t is

$$R = kt + R_\infty. \tag{B2}$$

The fitting curves of R and t is shown in Fig. B1(a) and the coefficient of determination R^2 is 0.7995. The coefficient of determination R^2 indicates how well data fits the curves. When the value of R^2 is larger, the fitting result is better.

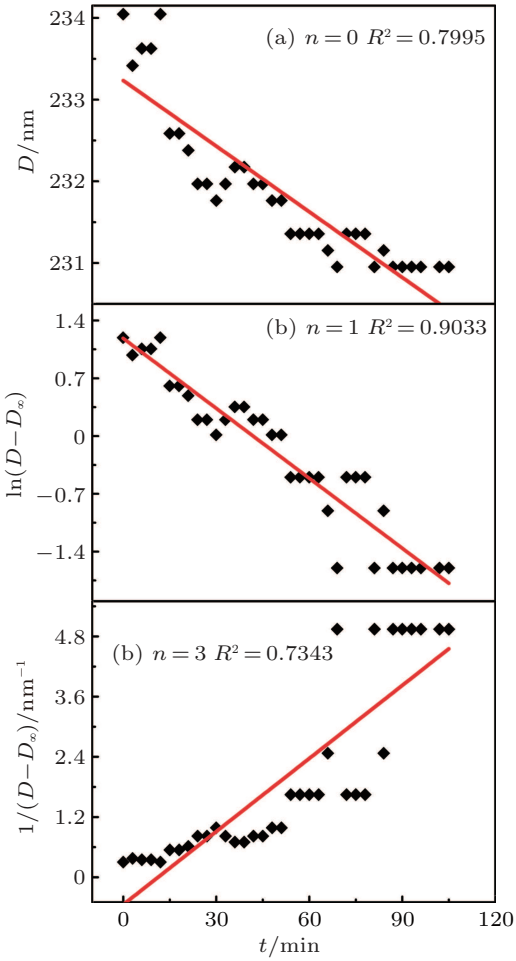


Fig. B1. (color online) Evolution of experimental data (black dot) and fitting curves (red line) with t when n is equal to (a) 0, (b) 1, and (c) 2.

When $n = 1$, equation (6) becomes Eq. (7). The fitting curves of $\ln(R - R_\infty)$ and t are shown in Fig. B1(b) and R^2 is 0.9033.

When $n = 2$, equation (6) becomes

$$v = k(R - R_\infty)^2 = \frac{\mathrm{d}R}{\mathrm{d}t}. \tag{B3}$$

Do integration of R and t, and the specific relationship between R and t is

$$\frac{1}{R - R_\infty} = kt + \text{cons}. \tag{B4}$$

The fitting curves of $1/(R - R_\infty)$ and t is shown in Fig. B1(c) and R^2 is 0.7343.

Comparing the above three cases, R^2 in the case of $n = 1$ is the largest. It indicates that the fitting result is much more appropriate when the parameter n is one. To further test the fitting results, correlation tests are done here. As there are finite pairs of data, the correlation coefficient is

$$\gamma = \frac{\sum[(x_i - \bar{x})(y_i - \bar{y})]}{\sqrt{\sum(x_i - \bar{x})^2 \sum(y_i - \bar{y})^2}}, \tag{B5}$$

where $\bar{x}$ and $\bar{y}$ are the average values. The correlation coefficient is a measure of the degree of linear dependence between two variables. The absolute value of γ ranges from 0 to 1. When $|\gamma|$ is larger, the correlation between data and fitting line is better. When $n = 0$, 1, 2, γ is 0.8974, 0.9519, and 0.8614, respectively. It indicates that the fitting is much more reasonable and reliable when $n = 1$.

Appendix C: estimation of the magnitude of forces

On one hand, as reported in Ref. [3], a unit cell in the film that is under stress σ_0 will have the stored elastic energy of $6\times2^{1/2}\sigma_0 R^2 \mathrm{d}r$, and the total attractive energy would be $(3/2)F_\mathrm{v}\mathrm{d}r$. The necessary condition for crack propagation is $6\times2^{1/2}\sigma_0 R^2\,\mathrm{d}r = (3/2)F_\mathrm{v}\,\mathrm{d}r$. On the other hand, to obtain the change of F_v when temperature varies from 318 K to 337 K, the relationship curve between van der Waals F_v and temperature T is plotted below according to Eq. (5.6) in Ref. [25]. From the curve, the change of F_v is 5%. Combining above two aspects, the 5% change of van der Waals can result to the difference between stored elastic energy and attractive energy, which can lead to the difference of deformation rate.

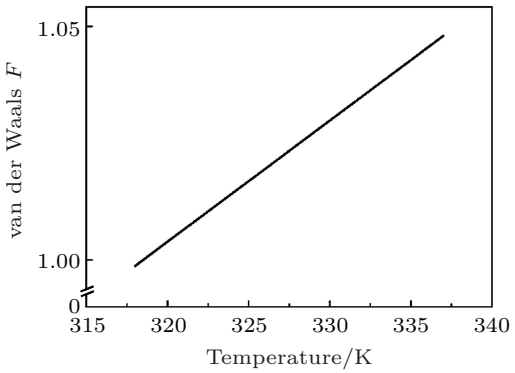


Fig. C1. Dependence of van der Waals F_v and temperature T from 318 K to 337 K.

For the reference, the magnitudes of F_v and σ_0 are estimated. According to Eqs. (5)–(7) in Ref. [3], van der Waals interaction F_v is

$$F_\mathrm{v} = \frac{A}{12Z_0^2}\left(R + \frac{a^2}{Z_0}\right) = \frac{A}{12Z_0^2}\left(R + \frac{0.191R^2}{Z_0}\right) \approx 10^{-7}\ \mathrm{N},$$

and the tensile stress σ_0 is

$$\sigma_0 = \frac{\sqrt{2}}{8R^2}F \approx 10^5\ \mathrm{Pa}.$$

Appendix D: final CCD images of crack under different temperatures

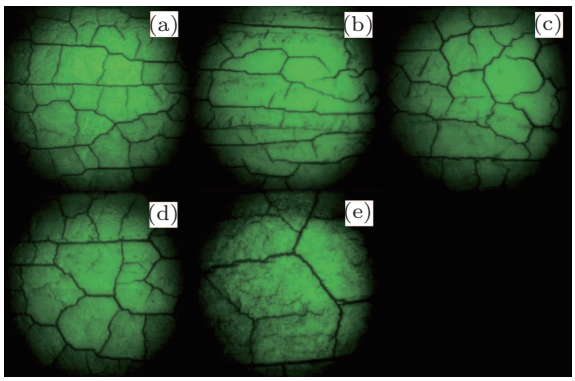


Fig. D1. (color online) The CCD images of CPCFs when the crack propagation stops under different temperatures: (a) 44.8 °C, (b) 47 °C, (c) 50.7 °C, (d) 57.6 °C, (e) 63.9 °C.

References

[1] Routh A F 2013 *Rep. Prog. Phys.* **76** 046603
[2] Huang Y, Zhou J, Su B, Shi L, Wang J, Chen S, Wang L, Zi J, Song Y and Jiang L 2012 *J. Am. Chem. Soc.* **134** 17053
[3] Cao H, Lan D, Wang Y, Volinsky A A, Duan L and Jiang H 2010 *Phys. Rev. E* **82** 031602
[4] Hartsuiker A and Vos W L 2008 *Langmuir* **24** 4670
[5] Singh K B and Tirumkudulu M S 2007 *Phys. Rev. Lett.* **98** 218302
[6] Lee W P and Routh A F 2006 *Ind. Eng. Chem. Res.* **45** 6996
[7] Tirumkudulu M S and Russel W B 2005 *Langmuir* **21** 4938
[8] Teh L K, Tan N K, Wong C C and Li S 2005 *Appl. Phys. A* **81** 1399
[9] Wong S, Kitaev V and Ozin G A 2003 *J. Am. Chem. Soc.* **125** 15589
[10] Velikov K P, van Dillen T, Polman A and van Blaaderen A 2002 *Appl. Phys. Lett.* **81** 838
[11] Shorlin K A, de Bruyn J R, Graham M and Morris S W 2000 *Phys. Rev. E* **61** 6950
[12] Hodges C S, Ding Y and Biggs S 2010 *J. Colloid Interface Sci.* **352** 99
[13] Tarafdar S and Sinha S 2008 *Ind. Eng. Chem. Res.* **47** 6459
[14] Ball P 2004 *Nat. Mater.* **3** 851
[15] Bucklow S 1999 *Stud. Conserv.* **44** 233
[16] Bucklow S 1997 *Stud. Conserv.* **42** 129
[17] Routh A F and Russel W B 1999 *Langmuir* **15** 7762
[18] Lin D, Wang J, Yang L, Luo Y, Li D and Meng Q 2014 *Langmuir* **30** 3949
[19] Wang J, Yang L, Lin D, Luo Y, Li D and Meng Q 2012 *J. Chem. Phys.* **137** 234111
[20] Yang L, Gao K, Luo Y, Luo J, Li D and Meng Q 2010 *Langmuir* **27** 1700
[21] Li J, Xue L, Wang Z and Han Y 2007 *Colloid. Polym. Sci.* **285** 1037
[22] Gates B, Park S H and Xia Y 2000 *Adv. Mater.* **12** 653
[23] Mazur S, Beckerbauer R and Buckholz J 1997 *Langmuir* **13** 4287
[24] López C, Vázquez L, Meseguer F, Mayoral R, Ocaña M and Miguez H 1997 *Superlattices Microstruct.* **22** 399
[25] Lifshitz E M 1956 *Soviet Phys.* **2** 73